Integration of Highly Sensitive Oxygenated Graphene With Aluminum Micro-Interdigitated Electrode Array Based Molecular Sensor for Detection of Aqueous Fluoride Anions

Mahesh Soni, Tarun Arora, Robin Khosla, Pawan Kumar, Ajay Soni, and Satinder K. Sharma

***Abstract*— High sensitivity and reliability of graphene oxide (GO) integrated with aluminum (Al) micro-interdigitated electrodes (μ-IDEs) patterned on p-Si for the detection of aqueous fluoride anion (F^-) is demonstrated. The strong molecular interaction, hydrogen bonding, and ionic conduction between the oxygen containing functional groups (epoxy (1, 2-ether), hydroxyl, carbonyl, and carboxyl) onto GO and F^- are investigated by electrical and optical techniques. The GO/Al (μ-IDEs)/p-Si sensor system shows ∼82% increase in the sensing signal for 0.1 ppm GO + F^- solution with respect to GO. The response of the sensor for 1, 10, 100, and 1000 ppm of GO + F^- solution shows almost 220, 415, 500, and 305 times increase in sensing signal with respect to GO. The significant enhancement in sensor response at lower concentration (0.1–100 ppm) of F^- is observed. However, at high concentration (1000 ppm) of F^-, the interlayer swelling and the expansion of GO dominate and result the reduction in sensing response of GO/Al (μ-IDEs)/p-Si sensor. The Fourier transform infrared spectroscopy (FT-IR) spectra show the decrease in –OH, C–O–C, and CLO absorption peaks of GO with an increasing aqueous F^- concentration, supporting the reduction in sensing response at 1000 ppm. The response of GO/Al (μ-IDEs)/p-Si sensor is favorable for use in graphene-based electronics sensors.**

***Index Terms*— F^- sensor, graphene oxide, mask-less lithography, micro-interdigitated electrodes, molecular interaction.**

I. Introduction

GRAPHENE oxide (GO) [1]–[3] and reduced graphene oxide (r-GO) [4], [5] 2D nano-materials are extensively incorporated to improve the prevailing electronic device performance and establishing novel functionalities in diverse range of disciplines [6]–[10]. The most striking feature includes, high surface to volume ratio, high carrier mobility, outstanding electrical and thermal conductivity [11], [12]. The existence of direct band gap in GO can be altered by oxidation process [13] and thus, the functionalized derivative emerged as a promising candidate especially for chemical sensor applications. The GO decorated with chemically reactive epoxy (C-O-C), hydroxyl (-OH) groups at basal plane and carboxyl (C=O-OH), carbonyl (C=O) groups at the edges [5], [13], [14] have proven their relevance for rapid and long-lasting proficiency to GO based sensor applications [8], [15], [16].

The detection (or removal) of toxic organic/inorganic pollutants present in (or from) natural sources of drinking water acquainted from industrial waste, drugs, nuclear plants have attracted an immense attention due to their direct impacts on the ecosystem [17]. Especially, the fluoride based pollutants in natural drinking water have imposed serious challenges to the human, animal health concerns and global plan of sustainable environment [18]. Although, aqueous fluoride anions (F^-, the smallest anion), is an essential element and plays an important role in the human/animal body, yet toxic in high concentrations [19]. The permissible range of F^- in natural drinking water as per World Health Organization (WHO) standard is 1.5 mg/L [20]. The high concentration of F^- in drinking water is one of the most prevalent severe health hazards across the globe. The high F^- intake results in adverse health effects, like gastric, kidney disorders, dental and skeletal fluorosis [17].

Recently, the synthesis and characterization of novel organic semiconductor sulfonamide-conjugated benzo-[2, 1-b: 3, 4-b]bithiophene and 4-(*tert*-butyldimethylsilyloxy)-N-butyl-naphthalimide (TBS-NA) is reported [21], [22]. The detection of aqueous F^- was based on optical NMR and colour change (from colourless to yellow) along with UV–Vis absorption spectral change. Besides this, ion-selective electrode and ion chromatography have also been investigated [23]. The reported techniques in literature for aqueous F^- detection are based on NMR, UV-Vis, chromatography which are hampered from low sensitivity, prolonged measurement time, detection in a specific range of wavelength [24]. The insufficient sensitivities and reliability based hindrance make above discussed techniques difficult to promote globally.

Therefore, a highly sensitive, reliable and low cost standard F^- sensor with cutting edge sensing material is immensely desired for keeping the F^- concentration within the WHO permissible standards. Nair *et al.* [25] presented sub-micrometer GO membranes resistant to liquid, vapour and gas flow,

Manuscript received September 21, 2015; accepted November 27, 2015. Date of publication December 7, 2015; date of current version February 8, 2016. This work was supported by the Department of Science and Technology through the Start-Up Research Grant Fast Track Young Scientist, India, under Grant SR/FTP/ETA-53/2012. The work of A. Soni and S. K. Sharma was supported by Indian Institute of Technology (IIT) Mandi, through the seed grant under the new faculty start up, Mandi, India. The associate editor coordinating the review of this paper and approving it for publication was Prof. Venkat R. Bhethanabotla. *(Corresponding author: Satinder K. Sharma.)*

M. Soni, T. Arora, R. Khosla, P. Kumar, and S. K. Sharma are with the School of Computing and Electrical Engineering, Indian Institute of Technology-Mandi, Mandi 175001, India (e-mail: satinder@iitmandi.ac.in).

A. Soni is with the School of Basic Sciences, Indian Institute of Technology-Mandi, Mandi 175001, India (e-mail: ajay@iitmandi.ac.in).

Digital Object Identifier 10.1109/JSEN.2015.2505782

including helium, but shows superpermeability to water molecules. Moreover, Borini *et al.* [8], Yao *et al.* [26], reported ultra fast humidity sensing devices based on the interaction of GO with water molecules.

To best of author's knowledge, it is the first report for detection of F^- based on integration of highly sensitive GO and Al-μ-IDEs. The electrical characterization is performed using simple conductance, impedance measurements and dielectric-constant variation using Keithley 4200 Semiconductor Characterization System (SCS). For electrical characterization, between the two electrodes one is used as a working (maintained at higher potential) and other is used as a relative (maintained at lower potential) electrode. The electrodes were connected to the Source Measure Unit (SMUs) of the SCS via tri-axial cables; similar approach was also opted in literature [26]–[29]. While, the reference solution was prepared and standardized separately.

In μ-IDEs, electrode material properties also play a vital role to meet the enhanced sensitivity and reliability of the MEMS based chemical sensors. The μ-IDEs electrode must have a high adhesion to the substrate, high melting point, intermediate thermal conductivity, capable of wire bonding for packaging, patterned by lift-off (for thickness $\geq$ 200 nm) and should be CMOS process compatible [30]. Aluminium (Al) metal offers the desired properties required for electrode material in MEMS based chemical sensors [30]. Anyhow, Al oxidises at low temperature and forms aluminium oxide (Al_2O_3), meanwhile it is highly sensitive for the removal of aqueous F^- owing to ion exchange formulation at the available active sites on the Al surface [18].

In the present work, a highly sensitive GO/Al (μ-IDEs)/p-Si sensor system consists of GO integrated with μ-IDEs array for aqueous F^- sensor application designed and fabricated on the basis of two important characteristics: first, the high interaction of F^- present in aqueous solution with GO as a sensing material result in variation of electrical impedance due to molecular interaction. Moreover, the large surface area of GO helps to enhance the surface loading of F^- and results in an excellent sensitivity and reliability. Secondly, the proposed fabrication of μ-IDEs array owing to safe, simple, inexpensive for mass production, ability to scale down the μ-IDEs helps to enhance GO/Al (μ-IDEs)/p-Si sensor sensitivity and consistency to wide domain.

The paper is organized as follows: the experimental detail including preparation of F^- stock solution, synthesis of GO, fabrication procedure for GO/Al (μ-IDEs)/p-Si sensor system is described in Section II. The sensing signal-voltage, Nyquist plot, capacitance-frequency characteristics along with the proposed model of the GO integrated with Al-μ-IDEs for detection of aqueous F^- is presented in Section III. Finally, Section IV summarizes the main findings and concludes the paper.

II. Experimental

A. Materials

Graphite, extra fine powder (particle size $<$ 50 μm, 99.999% pure), Sodium Nitrate ($NaNO_3$), Potassium permanganate ($KMnO_4$), Hydrogen Peroxide (H_2O_2), Hydrochloric acid (HCl), Sodium Fluoride (NaF) were purchased from Merck and Sulphuric acid (H_2SO_4) was procured from Fisher Scientific. De-ionized (DI) water with resistivity of 18.2 MΩ/cm was used for cleaning and solution preparation. Synthesis of GO was carried out using modified Hummers method [14] through oxidation of graphite.

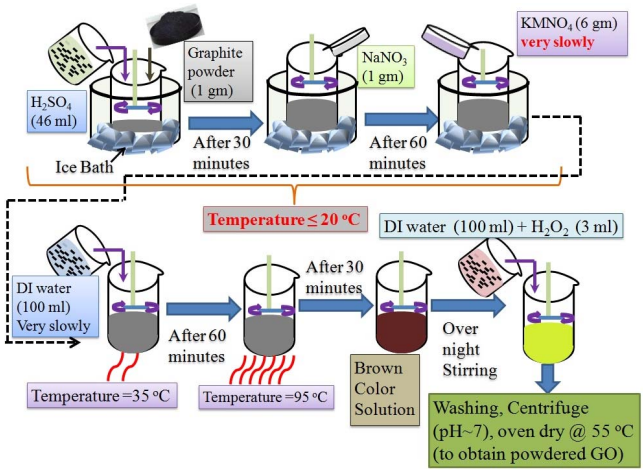

Fig. 1. Schematic of GO synthesis procedure from natural graphite based on Modified Hummers Method.

A stock solution of aqueous F^-, 1000 ppm was prepared by dissolution of 2.210 gm of NaF (Mw. 41.98871 g/Mol) in 1000 ml DI water. Likewise, the further dilutions were followed using the standard normality equation for F^- concentration in aqueous solution to be 100, 10, 1 and 0.1 ppm. In the present sensor investigations $\sim$ 300 μl solution of various F^- concentrations was filled in the PDMS reservoir (with dimensions 2.5*2.5*0.8 cm) and utilized for aqueous F^- sensing application.

B. Methodology for GO Preparation

Fig.1 shows the systematic procedure employed for the synthesis of GO (as a sensing precursor for F^- from graphite. A glass beaker (500 ml) was kept in an ice bath (0-5 °C). Graphite flakes (1 gm) along with conc. H_2SO_4 (46 ml) was poured into the beaker and stirred at 500 rpm for 30 minutes; stirring the solution, colour turns out to be dark grey. Later, $NaNO_3$ (1 gm) was added to the dark grey coloured solution, followed by stirring at 600 rpm for 60 minutes. In the next step, $KMnO_4$ (6 gm) was slowly added with due care that the temperature of the solution should not be more than 20 °C. Thereafter, the resultant solution was stirred at 600 rpm for 60 minutes. Afterward, the ice bath was removed and the temperature was slowly increased from 0-5 to 35°C along with continuous stirring for 60 minutes. Subsequently, the current solution was also diluted by slow addition of DI water (100 ml) with constant stirring for another 60 minutes. Ensuing this, the temperature was rapidly raised up to 95 °C and the precedent solution was stirred for 30 minutes, which resulted in the colour change from dark grey to brown. After that, the solution temperature was brought down to 25 °C and was kept for overnight stirring at 600 rpm. To terminate the reaction kinetics, the brown colour solution is finally treated with a

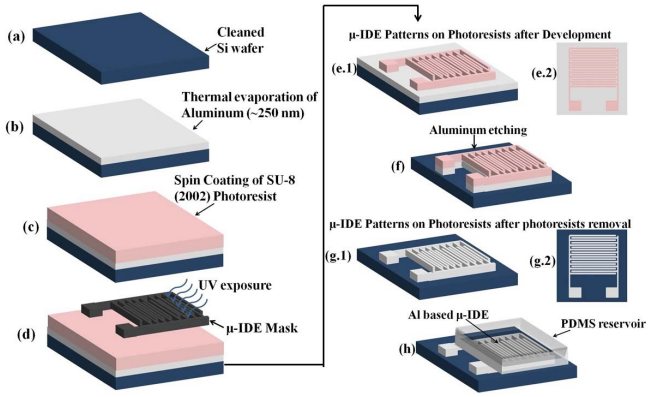

Fig. 2. Detailed description of the fabrication process of the μ-IDE structure and PDMS reservoir.

mixture of 100 ml DI water and 3 ml H_2O_2 (30%) which resulted in colour change from brown to greenish yellow.

Subsequently, the solution was then sonicated (Rivotek, 33 KHz) for 240 minutes and after that the solution was kept idle for 240 minutes (for sedimentation of heavy particulates). The remaining solution was poured to filter with vacuum filtration system. The final, filtrate obtained was washed using a gravity based centrifugation step: Initially, the solution was centrifuged at 3000 rpm for 5 minutes and the resulting mixture was washed separately with 3 wt% HCl. The preceding washing process was repeated twice. Hence forth, the resulted solution was repeatedly centrifuged at 5000 rpm for 7 minutes and washed with DI water until the pH of the solution turned to 7. Lastly, the resulted solution was kept in hot oven to dry at 55 °C until it disciple in powder form.

C. Fabrication of μ-IDEs Arrays for GO/Al (μ-IDE)/Si Sensor

p-Si wafers with <100> orientation were cleaned with: (i) sonication in acetone for 5 min, (ii) methanol dip 1 min, (iii) IPA rinse, (iv) dried using dry N_2 gas and (v) kept for dehydration bake at 200 °C for 5 min. The samples were allowed to cool down till room temperature (RT). Al thin film (∼250 nm) was deposited over the Si samples using thermal evaporator under high vacuum (pressure of $\sim 8.8 \times 10^{-7}$ m Bar) as shown in Fig. 2 (b). After that the SU-8 (2002, Micro-Chem) photoresist was spin coated on the Al/Si samples using the two step method: (i) The samples were spin coated at 500 rpm for 10 sec for uniformly spreading the photo resist over the substrate and (ii) immediately to 3000 rpm for 30 sec to deposit uniform photo resist film, at an acceleration of 100 and 300 rpm/sec respectively (Fig. 2(c)). The samples were then subjected to pre-exposure bake (PB) from RT to 95 °C for 10 min and after PB, the samples were allowed to cool down to RT. After the PB process, the samples were exposed using Maskless Optical Lithography (Intelligent Micro Patterning) to pattern μ-IDE structure and the samples were then subjected to post exposure bake (PEB) from RT to 105 °C for 10 min. Thereafter, samples were developed using SU-8 developer (Micro-Chem), for 1 min followed by IPA rinse and dried using dry N_2 gas (cross sectional view shown in Fig. 2 (e.1) and top view in Fig. 2 (e.2)) and performed the hard bake at 150 °C for 20 min. In order to get μ-IDE patterns, samples were etched through Al etchant (DI water, Acetic Acid, Nitric Acid, Ortho phosphoric acid, in the ratio 1:2:2:10) for 5-7 minutes at 35 °C with constant stirring of 100 rpm and were washed with DI water couple of times, (cross sectional view shown in Fig. 2 (f)). The undesirable SU-8 was removed by dipping the samples in N-Methyl-2-pyrrolidone (NMP), at 75 °C for 38-40 min under constant stirring of 100 rpm, and rinsed by IPA, DI water back to back. Hence, the dimensional parameters of the μ-IDE array for the present study is width (W) = spacing (D) = 300 μm, length (L) = 10 mm and number of μ electrode fingers (N) = 17 (cross sectional view shown in Fig. 2 (g.1) and top view in Fig. 2 (g.2)).

D. Fabrication of Integrated Reservoir for GO/Al (μ-IDE)/Si Sensor

The integrated PDMS reservoir for electrochemical sensing application was prepared using Sylgard 184 base and curing agent in the ratio of (10:1). 10 gm of base was mechanically stirred with 1 gm of the curing agent in a beaker for 15 minutes and subsequently degassing of air bubbles were performed. Further, the PDMS blend was slowly poured into a petri dish over a mould to attain the desired shape, thickness and cured inside the oven at 70 °C for 240 minutes to form a solid. After that, the PDMS based reservoir was carefully peeled off from mould using a dissection blade, and was placed over the Al-μ-IDEs structure. Fig. 2 (h) shows the cross-sectional view of the Al based μ-IDEs with PDMS reservoir.

Although the electrode fabrication in the same batch was used for all the sets of measurement, but due to lack of industrial scale process control in the lab, it leads to variation in impedance of the electrodes. However after the drop cast of GO, the offset for the samples were compensated and were adjusted accordingly.

III. Results and Discussion

Sensing signal-voltage characteristics (I-V) curves as a function of different concentration of GO 1 mg/ml with GO + F^- (0.1-1000 ppm) and 0.25 mg/ml with GO + F^-(0.1-100 ppm) is shown in Fig 3 (a) and Fig. 3 (b) respectively. The F^- dissociation mechanism from NaF in the aqueous solution is given by following Eq.:

$$NaF \leftrightarrow Na^+ + F^- \quad (1)$$

$$F^- + H_2O \leftrightarrow HF + OH^- \quad (2)$$

$$HF + H_2O \leftrightarrow H_3O^+ + F^- \quad (3)$$

$$Na^+ + OH^- \leftrightarrow NaOH \quad (4)$$

As shown in Eq. (1)-(4), NaF dissociate into sodium cations (Na^+) and fluoride anions (F^-) followed by the formation of a weak acid (HF) due to the reaction between F^- and H_2O molecules. Finally, this weak acid formulation results the strong conjugate base (F^-), and a strong conjugate acid (H_3O^+) in the aqueous solutions as shown in Eq. (3) [31]. The Na^+ may react with the OH^- and form NaOH.

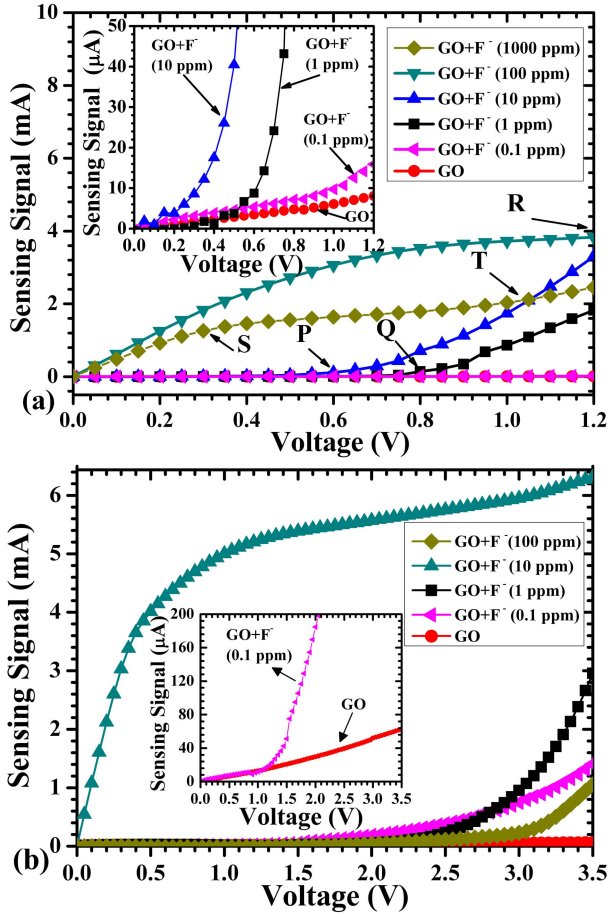

Fig. 3. Sensing signal-Voltage (I-V) characteristics for Al-μ-IDE with GO and GO+F^- as a function of GO concentration of (a) 1mg/ml, with the GO+F^- in the range of 0.1-1000 ppm up to 1.2 V (b) 0.25 mg/ml, with the GO+F^- in the range of 0.1-100 ppm up to 3.5 V. Inset shows the zoom in I-V curves for GO and GO+F^-.

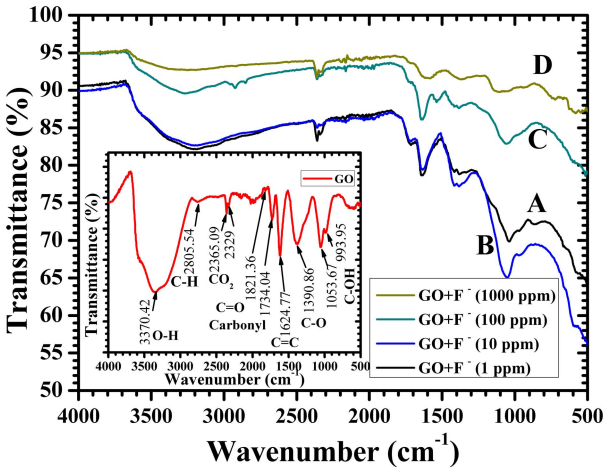

Fig. 4. FT-IR transmittance spectrum as a function of GO+F^- concentration ranging from 1-1000 ppm. The inset shows the FT-IR transmittance spectra for GO powder along with the active functional groups attached to it. FT-IR spectrum labelled with A, B, C, D represents the GO+F^- concentration of 1, 10, 100 and 1000 ppm respectively.

From the inset of Fig. 3(a), the I-V characteristics curve for reference GO (without F^- varies from 0 to $\sim$ 8 μA. While for F^- aqueous solution of 0.1 ppm, the sensing signal varies from 0 to $\sim$ 14.5 μA. It indicates a substantial increase in sensor response signal $\sim$ 82 %. Furthermore, for F^- solution of 1 ppm, the sensing signal varies slightly up to "Q" (0.8 V) $\sim$ 0.142 mA. Ahead of "Q", sensor signal varies linearly and advances to $\sim$ 1.79 mA at 1.2 V. Correspondingly, for F^- aqueous solution of 10 ppm, the sensor response varies trivially till "P" (0.6 V) $\sim$ 0.112 mA, whereas afterwards "P", sensor response signal varies linearly and progresses to $\sim$ 3.3 mA at 1.2 V.

In contrast to this, for F^- aqueous solution of 100 ppm, the sensing signal increase is noticed at the low voltage and finally saturates at 1.2 V with maxima of $\sim$ 4 mA. Therefore, this perceptible variation in GO/Al (μ-IDEs)/p-Si sensor response signal for various F^- concentrations of 1, 10, 100 ppm, are $\sim$220, $\sim$415, $\sim$500 fold increase with respect to reference GO/Al (μ-IDEs)/p-Si sensor system (without F^-) at "R" (1.2 V). Whereas, on increasing the F^- concentration beyond 100 ppm, followed the similar variation of sensing signal till point "S" ($\sim$0.3 V) up to $\sim$ 1.18 mA as discussed earlier. However, the sensor signal for F^- solution of 1000 ppm shows 50 % reduction as compared with the 100 ppm ("T" ($\sim$1.04 V)). Besides this, the measured sensing signal for F^- solution of 1000 ppm is astonishingly lower than 10 ppm beyond point "T". The computed slope for GO/Al (μ-IDEs)/p-Si sensor signals are 6.667 & 12.08 μA/V for GO (reference) and GO+F^- solution of 0.1 ppm. Similarly, the calculated slope for the sensor signal of aqueous F^- solution of 1, 10, 100 ppm are 1.49, 2.75, 3.33 mA/V, respectively. It indicates that there is a considerably increase in GO/Al (μ-IDEs)/p-Si sensor response and voltage shift towards lower voltage (from 0.8 to 0.6 V) with the variation of F^- concentration (1 to 10 ppm). It attributes that there is substantial increase in GO/Al (μ-IDEs)/p-Si conductance with variation of F^- aqueous solution, due to the molecular interactions with accessible higher energy binding sites of GO [5], [13]. The binding sites includes vacancies, active structural defects, available oxygen containing functional groups present on reactive epoxy (C-O-C), hydroxyl (-OH) at basal plane and carboxyl (C=O-OH), carbonyl (C=O) at the edges [5], [13], [14].

While the reduction of sensor signal for 1000 ppm, represents the saturation or lesser number of binding sites (oxygen containing functional groups) present onto GO. Moreover, the F^- present in aqueous solution might be permeable by GO, interacts with Al μ-IDEs and results the reduction in sensor signal due to strong affinity of aqueous F^- with Al [18].

Additionally, as shown in Fig. 3 (b), on reducing the concentration of GO from 1mg/ml to 0.25 mg/ml, the sensor response to F^- in the range of 0.1-10 ppm at 3.5 V. Hence, for low concentration of GO, the sensing range of the sensor reduces and the sensor operates at higher voltage.

In order to confirm the availability of active oxygen containing functional groups in GO for F^- detection in aqueous solution, FT-IR characterization of GO powder was performed. Fig. 4 inset shows the FT-IR spectra of GO and the availability of characteristic hydroxyl group (-OH) absorption

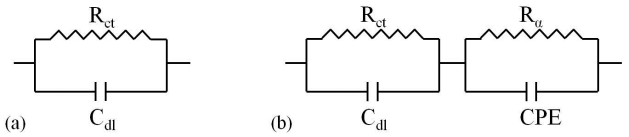

Fig. 5. Equivalent circuit for (a) GO integrated with μ-IDEs and (b) GO/Al (μ-IDEs)/p-Si with sensing solution of 0.1-1000 ppm.

band peaks at 3370.42 cm^{-1}, carbon–carbon (C=C) peak at 1624.77 cm^{-1}. As well, the existence of epoxy (C–O–C) stretching and carbonyl groups (CLO) of carboxylic derivatives stretching at 1053.67 & 993.95 cm^{-1} and 1821.36 & 1734.04 cm^{-1} [5], [13], [14]. Fig. 4 shows the FT-IR transmittance spectrum for GO+F^- powder 1-1000 ppm. The transmittance spectra show a significant decrease in absorption intensity with the increase in F^-; GO+F^- 1 ppm (curve "A"), 10 ppm (curve "B"), and 100 ppm (curve "C"). The decrease in the characteristic absorption peaks for functional groups attached to GO attributes to adsorption of F^- on the active binding site in GO. Moreover, for F^- concentration of 1000 ppm (curve "D"), the FT-IR resembles almost a flat spectra, attributing to the saturation of active binding sites in GO for F^- concentration of 1000 ppm.

The intensity of the FT-IR spectra mostly decreases around 3300 and 1700 cm^{-1} which attributes to the presence of hydroxyl (OH) functional group and carboxylic derivatives in GO. With the increase in the concentration of F^- the presence of OH functional groups and carboxylic derivatives decreases leading to reduction in the absorption peak intensity. Additionally, there is no shift in the peak positions of FT-IR spectra.

The absorption intensity maxima are noticed for GO+F^- of 1 ppm as compared with GO+F^- of 10 ppm for wavenumber ranging from 4000 to 1500 cm^{-1}. However, the region in the FT-IR spectra where absorption intensity peak is more for GO+F^- 10 ppm as compared with GO+F^- 1 ppm (without any shift in the peak position) may be attributed to the fingerprint region [32], [33]. Fingerprint region in the FT-IR spectrum is the region when the wavenumber is below 1500 cm^{-1} (from about 1500 to 500 cm^{-1}). The fingerprint region consists of very complicated series of absorptions band peaks like C-C, C-O, like in alcohols, ethers, esters, etc [32]. On the other hand in the finger print region, it is difficult to have the same FT-IR spectrum for any two compounds (except enantiomers). Indeed we could identify the alkyl halide (Carbon-Fluoride) stretching frequency around 1400-1000 cm^{-1} in the FT-IR spectra with the addition of the fluoride ion proving the adsorption of F^- onto the surface of GO.

In order to investigate the sensing behaviour of chemical sensors, the characteristics of Nyquist Plots with one or more semicircles has emerged as a useful analytical tool [34]. In the Nyquist Plots the impedance spectrum of fabricated GO/μ-IDEs/p-Si sensor system for F^- sensing application can be modelled by the parallel arrangement of resistance and capacitance. The Nyquist plots interpretation at different sensing stages for F^- interaction with the fabricated GO/Al (μ-IDEs)/p-Si sensor system can be described by the equivalent circuit as shown in Fig. 5.

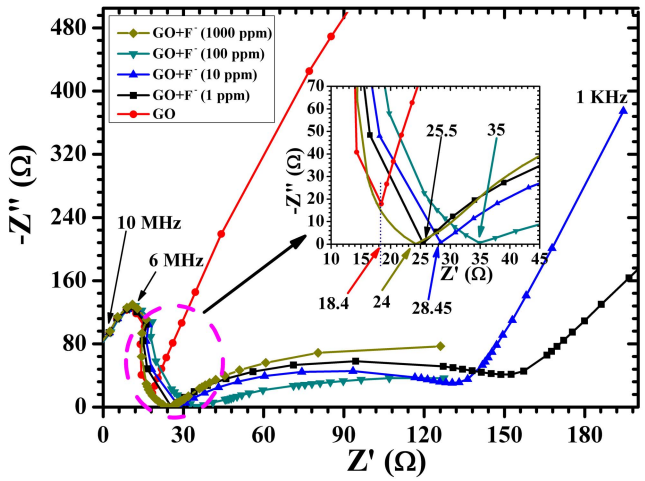

Fig. 6. Nyquist plot (–Z″ vs Z′ (Ω)) for μ-IDEs with GO and GO+F^- from 10M-1KHz, with F^- concentration ranging from 1-1000 ppm. Inset shows the zoom in nyquist plot for high frequency (Z′ in the range 15-45 Ω) with GO and variation in F^- concentration.

In the Nyquist Plots (Fig. 6), the diameter of the 1st semicircles at high frequency represents the interfacial charge transfer resistance (R_{ct}) and double layer capacitance (C_{dl}) of the GO/Al (μ-IDEs)/p-Si sensor system, as shown in Fig. 5 (a). The presence of second semicircle at lower frequency implies the formation of an additional layer between the Al-μ-IDEs and GO after the drop cast of aqueous F^- solution. As expected, there is likelihood for the formation of adsorbent layer and self-assembled layer of aqueous F^- solution onto GO/Al (μ-IDEs)/p-Si sensor system. The first layer classified as the interfacial layer (IL) formulated from the parallel combination of R_{ct} and C_{dl} as shown in Fig. 5(b). While the second, self-assembled layer (SAL) christened as the inner sub-layer composed of a constant resistance (R_α) and a constant phase element (CPE), as indicated in Fig. 5(b) [6], [34]. Although the computed –Z″ and Z′ (Ω) represent the overall impedance of aqueous F^- solution onto GO/Al (μ-IDEs)/p-Si sensor system for combined effect of IL and SAL. Fig. 6 shows the Nyquist plot of impedance spectra for GO/Al μ-IDEs/p-Si sensor system for F^- concentration of 1-1000 ppm. As revealed, all impedance spectrums consist of two semicircles apart from GO reference measured at 30 mV (RMS).

As shown in Fig. 6, impedance spectra, at higher frequencies, the diameter of the 1st semicircles as marked with dashed circle for F^- concentration 1-1000 ppm represents the interfacial charge transfer resistance (R_{ct}) onto μ-IDEs from the aqueous F^- sensing solution. As shown in Fig. 6, that on varying F^- concentration from 1-1000 ppm, the diameter of the 1st semicircles appearing in the high frequency region is increasing with respect to reference GO. It features the apparent variation in the R_{ct} of GO/Al (μ-IDEs)/p-Si sensor system, which resists the charge transfer from the sensing solution to the Al-μ-IDEs [6]. The computed R_{ct} (Ω) for reference GO (without F^-, and GO+F^- in aqueous solution at 1, 10, 100 ppm are 18.4 and 25.5, 28.45, 35 Ω respectively. Besides this, the increase in semicircle diameter at high frequency in the impedance spectra is the consequence of

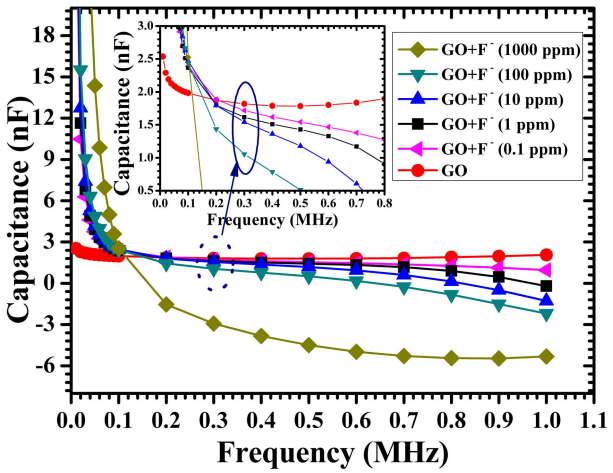

Fig. 7. Capacitance-Frequency (C-F) as a function of GO and GO+F^- concentration ranging from 0.1 -1000 ppm. Inset shows the zoom in C-F plot for in the frequency range 0 – 0.8 MHz with GO and variation in F^- concentration.

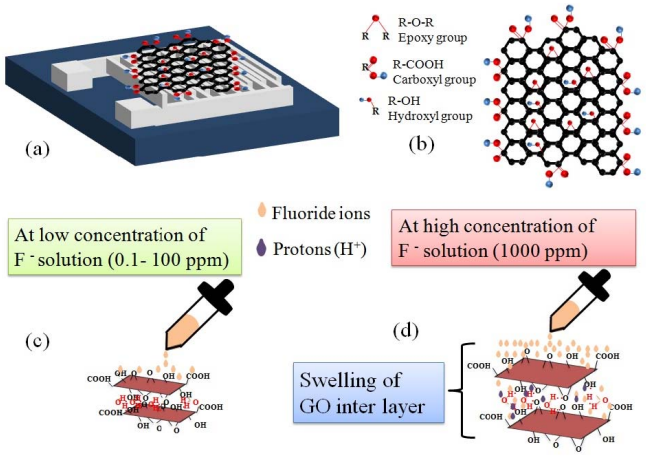

Fig. 8. Shows the (a) Integration of GO with Al based μ-IDEs, (b) monolayer GO sheet with the functional groups attached to its basal plane (epoxy, hydroxyl) and edges (carboxyl). The electrical interaction mechanism between fluoride ions present in aqueous solution and GO at (c) low concentration of F^- solution (0.1-100 ppm) and (d) high concentration of F^- solution (1000 ppm).

F^- molecules adsorption onto the active oxygen comprehending functional sites of epoxy, hydroxyl, carbonyl, carboxyl available in GO [5], [13]. Whereas, beyond 100 ppm, the R_{ct} magnitude should remain constant (due to saturation in bonding sites), although owing to high permeability of GO membranes to aqueous F^- molecules, the F^- penetrates the GO film. As a result, degrades the Al-μ-IDEs owing to the strong affinity of F^- for Al resulting in lower R_{ct} values [R_{ct} (=24 Ω)] [17], [18].

Fig. 7 shows the variation of Capacitance vs. Frequency (C-F) characteristics as a function of aqueous F^- solution ranging from 0.1-1000 ppm for fabricated GO/Al (μ-IDEs)/p-Si sensor system. The maximum capacitance measured for reference GO is $\sim$ 2.5 nF and tends to decrease with increase in frequency as shown in Fig. 7 and finally saturates at $\sim$2nF.

While, the measured capacitance of GO/Al (μ-IDEs)/p-Si sensor system decreases exponentially with frequency as a function of different concentration of F^- sensing solution ranging from 0.1-1000 ppm (as depicted in inset of Fig. 7). The computed capacitance for reference GO and GO+F^- of 0.1, 1, 10, 100 ppm are 1.8 nF and 1.73, 1.64, 1.55, 1.05 nF respectively at 0.3 MHz. Though, for F^- solution of 1000 ppm, the computed capacitance decreases exponentially and approaches to negative value. Additionally, the decrease in capacitance with the increasing concentration of aqueous F^- solution supports the increase in sensor signal with increasing fluoride ion aqueous solution (0.1-100 ppm). It indicates that as the measurement frequency increases, there might be more charge flow across the Al-μ-IDEs in a given time and results the increase in sensing signal.

As discussed and observed from the I-V, C-F, $-Z''$ vs Z' (Ω)) characteristic curves for F^- detection based on GO/Al μ-IDEs/p-Si sensor system, the sensitivity is strongly dependent on the amount of adsorbed/desorbed aqueous fluoride molecules onto the available binding sites in GO at low concentration 0.1-100 ppm (similar resemblance from FT-IR spectra for GO+F^- (1-100 ppm)).

Though, the F^- present in the aqueous solution are probably adsorbed on the active hydrophilic groups (mainly carboxylic at edges and hydroxyl at basal plane) as presented in schematic of the Fig. 8 (a) & (b) in GO through hydrogen and molecular bonding. Protons (H^+ generated as a result of the reaction of aqueous F^- with the hydroxyl of GO interaction with excess water molecules to form a strong conjugate acid H_3O^+ [2], [26]. These aqueous F^- are adsorbed on the GO surface and do not penetrate the GO film, hence the internal stress of the GO film is unaffected as shown in proposed model of Fig. 8 (c). On account of low concentration (0.1-100 ppm) of aqueous F^- solution, the functional sites in GO surface are adequate to form hydrogen and molecular bonding, results the increase in sensing signal. Furthermore, the adsorption of F^- onto GO surface results the increase in charge transfer resistance.

On the other hand, at higher concentration of F^- (1000 ppm), remarkable variation in the I-V, C-F, $-Z''$ vs Z' (Ω) characteristics for GO/Al (μ-IDEs)/p-Si sensor system is observed as shown in Fig. 3, 6 & 7. This considerable variation is attributed to the hydrogen bonding interaction between the aqueous F^- and the GO layers. The interaction leads to GO inter layer swelling and expansion [26] as shown in proposed model of Fig. 8 (d). The inter layer swelling and expansion in the GO significantly increases the inter layer distance and deteriorates the conductivity of GO sensing film [8], [26]. Thus, the decrease in conductivity of GO/Al (μ-IDEs)/p-Si sensor contributes to the reduction in response signal. Likewise, there is an increase in transfer of charge from the sensing solution to the μ-IDEs, the R_{ct} value for high concentration of F^- is reduced, and the measured capacitance for the GO/Al (μ-IDEs)/p-Si sensor is negative. The negative capacitance observed for GO/Al (μ-IDEs)/p-Si sensor system can be predominantly due to high conductivity of aqueous F^- solution and strong inductive effect of GO/Al (μ-IDEs)/p-Si sensor. Fig. 9 shows the variation of

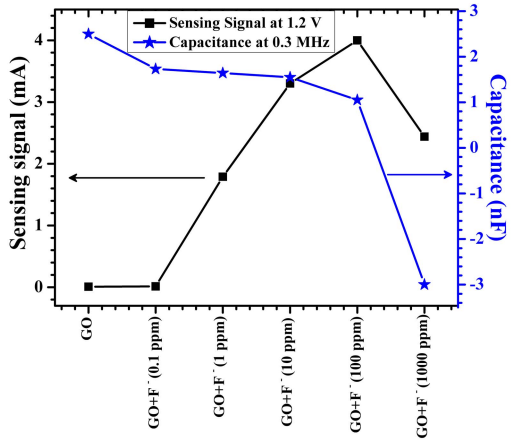

Fig. 9. Sensing signal and Capacitance variation with the change in F^- concentration from 0.1-1000 ppm.

GO/Al (μ-IDEs)/p-Si sensor signal (measured at 1.2 V) and capacitance (measured at 0.3 MHz) with the varying aqueous F^- solution from 0.1-1000 ppm. As shown in the Fig. 9 for reference GO (without F^-, the response signal minima and capacitance maxima are measured $\sim$8 μA and $\sim$2.5 nF. While, as the aqueous F^- concentration increases from 0.1 to 100 ppm, the response signal maxima and capacitance minima measured at 100 ppm is 4 mA at 1.2 V and 1.05 nF at 0.3 MHz, respectively. However, for aqueous F^- solution of 1000 ppm the sensor signal of GO/Al (μ-IDEs)/p-Si system is reduced to 2.44 mA and the capacitance is ~ -3 nF.

IV. Conclusion

This work demonstrates the successful integration of highly sensitive GO with optimum designed Al based μ-IDEs for GO/Al (μ-IDE)/p-Si sensor system for the detection of aqueous F^-. The proposed sensing system is capable of sensing the F^- concentration in the range of 0.1-100 ppm. The F^- present in the aqueous solution are adsorbed on the functional sites (epoxy, hydroxyl, carbonyl, carboxylic) available in GO and thus results in the increase of sensitivity. As a result, the GO/Al (μ-IDEs)/p-Si based sensor, with low cost, low power and easy fabrication, as well as scalable properties, showed great potential for ultrasensitive detection of fluoride ions present in the aqueous solution.

References

[1] F. Chen *et al.*, "Ethanol-assisted graphene oxide-based thin film formation at pentane-water interface," *Langmuir*, vol. 27, no. 15, pp. 9174–9181, Aug. 2011.

[2] A. M. Dimiev and J. M. Tour, "Mechanism of graphene oxide formation," *ACS Nano*, vol. 8, no. 3, pp. 3060–3068, 2014.

[3] S. K. Hong, J. E. Kim, S. O. Kim, S.-Y. Choi, and B. J. Cho, "Flexible resistive switching memory device based on graphene oxide," *IEEE Electron Device Lett.*, vol. 31, no. 9, pp. 1005–1007, Sep. 2010.

[4] Z. Bo *et al.*, "Green preparation of reduced graphene oxide for sensing and energy storage applications," *Sci. Rep.*, vol. 4, Apr. 2014, Art. ID 4684.

[5] F. Liu, R. Huo, X. Huang, Q. Lei, and P. Jiang, "Crystalline properties, dielectric response and thermal stability of in-situ reduced graphene oxide/poly(vinylidene fluoride) nanocomposites," *IEEE Trans. Dielectr. Electr. Insul.*, vol. 21, no. 4, pp. 1446–1454, Aug. 2014.

[6] J.-C. Chou, C.-H. Huang, Y.-H. Liao, S.-W. Chuang, L.-H. Tai, and Y.-H. Nien, "Effect of different graphene oxide contents on dye-sensitized solar cells," *IEEE J. Photovolt.*, vol. 5, no. 4, pp. 1106–1112, Jul. 2015.

[7] X. Feng *et al.*, "Preparation of graphene/polypyrrole composite film via electrodeposition for supercapacitors," *IEEE Trans. Nanotechnol.*, vol. 11, no. 6, pp. 1080–1086, Nov. 2012.

[8] S. Borini *et al.*, "Ultrafast graphene oxide humidity sensors," *ACS Nano*, vol. 7, no. 12, pp. 11166–11173, 2013.

[9] S. Jang, E. Hwang, J. H. Lee, H. S. Park, and J. H. Cho, "Graphene–graphene oxide floating gate transistor memory," *Small*, vol. 11, no. 3, pp. 311–318, Jan. 2015.

[10] H. Liang, Y. Bu, J. Zhang, Z. Cao, and A. Liang, "Graphene oxide film as solid lubricant," *ACS Appl. Mater. Interfaces*, vol. 5, no. 13, pp. 6369–6375, Jul. 2013.

[11] O. C. Compton and S. T. Nguyen, "Graphene oxide, highly reduced graphene oxide, and graphene: Versatile building blocks for carbon-based materials," *Small*, vol. 6, no. 6, pp. 711–723, Mar. 2010.

[12] W. Gao *et al.*, "Direct laser writing of micro-supercapacitors on hydrated graphite oxide films," *Nature Nanotechnol.*, vol. 6, no. 8, pp. 496–500, 2011.

[13] K. Krishnamoorthy, M. Veerapandian, K. Yun, and S.-J. Kim, "The chemical and structural analysis of graphene oxide with different degrees of oxidation," *Carbon*, vol. 53, pp. 38–49, Mar. 2013.

[14] B. Paulchamy and J. Jaya, "A simple approach to stepwise synthesis of graphene oxide nanomaterial," *J. Nanomed. Nanotechnol.*, vol. 6, no. 253, pp. 1000253, 2015.

[15] S. Basu and P. Bhattacharyya, "Recent developments on graphene and graphene oxide based solid state gas sensors," *Sens. Actuators B, Chem.*, vol. 173, pp. 1–21, Oct. 2012.

[16] N. Hu *et al.*, "Ultrafast and sensitive room temperature NH_3 gas sensors based on chemically reduced graphene oxide," *Nanotechnology*, vol. 25, no. 2, p. 025502, 2014.

[17] R. Sinha, A. Singh, and S. Mathur, "Multiobjective optimization for minimum residual fluoride and specific energy in electrocoagulation process," in *Desalination Water Treatment*. New York, NY, USA: Taylor & Francis, 2014, pp. 1–11.

[18] R. Sinha, S. Mathur, and U. Brighu, "Aluminium removal from water after defluoridation with the electrocoagulation process," *Environ. Technol.*, vol. 36, no. 21, pp. 2724–2731, 2015.

[19] F. Wang *et al.*, "A highly selective fluorescent sensor for fluoride in aqueous solution based on the inhibition of excited-state intramolecular proton transfer," *Sens. Actuators B, Chem.*, vol. 146, pp. 260–265, Apr. 2010.

[20] B. Kemer, D. Ozdes, A. Gundogdu, V. N. Bulut, C. Duran, and M. Soylak, "Removal of fluoride ions from aqueous solution by waste mud," *J. Hazardous Mater.*, vol. 168, pp. 888–894, Sep. 2009.

[21] H. Aboubakr, H. Brisset, O. Siri, and J.-M. Raimundo, "Highly specific and reversible fluoride sensor based on an organic semiconductor," *Anal. Chem.*, vol. 85, no. 20, pp. 9968–9974, 2013.

[22] R. Hu *et al.*, "A rapid aqueous fluoride ion sensor with dual output modes," *Angew. Chem. Int. Ed.*, vol. 49, no. 29, pp. 4915–4918, 2010.

[23] J. Ren, Z. Wu, Y. Zhou, Y. Li, and Z. Xu, "Colorimetric fluoride sensor based on 1,8-naphthalimide derivatives," *Dyes Pigments*, vol. 91, pp. 442–445, Dec. 2011.

[24] I. W. Kimaru, *Characterization of Chiral Interactions by Fluorescence Anisotropy and Development of Fluorescence Sensors for Recognition of Molecular Species*. Ann Arbor, MI, USA: ProQuest, 2006.

[25] R. R. Nair, H. A. Wu, P. N. Jayaram, I. V. Grigorieva, and A. K. Geim, "Unimpeded permeation of water through helium-leak–tight graphene-based membranes," *Science*, vol. 335, no. 6067, pp. 442–444, 2012.

[26] Y. Yao, X. Chen, J. Zhu, B. Zeng, Z. Wu, and X. Li, "The effect of ambient humidity on the electrical properties of graphene oxide films," *Nanosc. Res. Lett.*, vol. 7, no. 363, pp. 1–7, 2012.

[27] M. M. Rahman and A. M. Asiri, "Development of ionic-sensor based on sono-chemically prepared low-dimensional β-Fe_2O_3 nanoparticles onto flat-gold electrodes by an electrochemical approach," *Sens. Bio-Sens. Res.*, vol. 4, pp. 109–117, Jun. 2015.

[28] A. K. M. Muaz, U. Hashim, W.-W. Liu, F. Ibrahim, K. L. Thong, and M. S. Mohktar, "Fabrication of interdigitated electrodes (IDE's) by conventional photolithography technique for pH measurement using micro-gap structure," in *Proc. IEEE Conf. Biomed. Eng. Sci. (IECBES)*, Dec. 2014, pp. 146–150.

[29] J. Huang, S. Virji, B. H. Weiller, and R. B. Kaner, "Polyaniline nanofibers: Facile synthesis and chemical sensors," *J. Amer. Chem. Soc.*, vol. 125, no. 2, pp. 314–315, 2003.

[30] J. Laconte, D. Flandre, and J.-P. Raskin, "Gas sensors on microhotplate," in *Micromachined Thin-Film Sensors for SOI-CMOS Co-Integration*. Springer, 2006, pp. 195–196.
[31] W. L. Masterton and C. N. Hurley, *Chemistry: Principles and Reactions*. Boston, MA, USA: Cengage Learning, 2015.
[32] L. D. S. Yadav, "Infrared spectroscopy," in *Organic Spectroscopy*. Springer, 2013, pp. 92–93.
[33] H. Amrania, A. P. McCrow, M. R. Matthews, S. G. Kazarian, M. K. Kuimova, and C. C. Phillips, "Ultrafast infrared chemical imaging of live cells," *Chem. Sci.*, vol. 2, no. 1, pp. 107–111, 2011.
[34] R. Ohno *et al.*, "Electrochemical impedance spectroscopy biosensor with interdigitated electrode for detection of human immunoglobulin A," *Biosensors Bioelectron.*, vol. 40, pp. 422–426, Feb. 2013.

Mahesh Soni was born in Durg, India, in 1988. He received the bachelor's degree in electronics and telecommunication from Chhattisgarh Swami Vivekananda Technical University, Bhilai, India, in 2010, and the master's in VLSI design from NIT Jaipur, in 2012. He is currently pursuing the Ph.D. degree with the Indian Institute of Technology (IIT) Mandi, India. Since 2014, he has been working with S. K. Sharma and A. Soni at IIT Mandi on graphene-based FETs.

His research interest includes memory devices and sensors based on graphene and its derivatives for next-generation optimal power high-performance nanoelectronic regime devices.

Tarun Arora was born in Delhi, India, in 1991. He received the bachelor's degree in electronics and communication from the Accurate Institute of Management and Technology, Greater Noida, India, in 2012. He is currently pursuing the Ph.D. degree with the Indian Institute of Technology (IIT) Mandi, India. Since 2014, he has been working with S. K. Sharma at IIT Mandi on integrated heat sink using microfluidics. His research interest includes flexible memory devices and MEMS devices for sensors and integrated heat sink application.

Robin Khosla was born in Punjab, India, in 1989. He received the B.Tech. degree in electronics and communication engineering and the M.Tech. degree in VLSI design from Punjab Technical University, Punjab, in 2011 and 2013, respectively. He is currently pursuing the Ph.D. degree with the School of Computing and Electrical Engineering, Indian Institute of Technology (IIT)-Mandi, India.

His research interests include fabrication, characterization and reliability of high-k dielectrics for CMOS and nonvolatile memory applications.

Pawan Kumar was born in Himachal Pradesh, India, in 1986. He received the B.Sc. and M.Sc. degrees from Himachal Pradesh University, Shimla, India, in 2007 and 2009, respectively, and the Ph.D. degree in physics from Jaypee University of Information Technology, Waknaghat, India, in 2015.

He is currently a Senior Project Scientist with the School of Computing and Electrical Engineering, Indian Institute of Technology (IIT)-Mandi, Mandi, India. His research interests include applications of scanning probe microscopy characterizations of thin-oxide films and investigations of the surfaces and surface properties of nanomaterials.

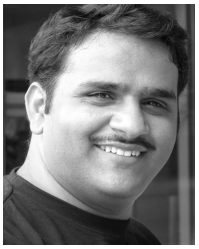

Ajay Soni received the Ph.D. degree from the UGC DAE Consortium for Scientific Research, Indore, India, in 2009, on the study of physical properties of nanomaterials. From 2009 to 2011, he was a Post-Doctoral Research Fellow with Nanyang Technological University, Singapore, and from 2011 to 2013, as a Post-Doctoral Research Fellow with National University of Singapore, Singapore. He is currently an Assistant Professor with the School of Basic Sciences, Indian Institute of Technology Mandi, India.

His current research interests includes nanomaterials and mesoscopic physics, low-temperature physics, thermoelectric, and optoelectronic chalcogenide materials.

Satinder K. Sharma was born in Himachal Pradesh, India, in 1978. He received the M.S. degree in physics (Electronic Science) from Himachal Pradesh University, Shimla, India, in 2002, and the Ph.D. degree from the Department of Electronic Science, Kurukshetra University, Kurukshetra, India, in 2007. His Ph.D. thesis was on silicon-based gate dielectric materials for VLSI/ULSI technology.

From 2007 to 2010, he was a Post-Doctoral Fellow at the DST Unit on Nanosciences and Nanotechnology, Dept. CHE, Indian Institute of Technology (IIT) Kanpur, Kanpur, India. From 2010 to 2012, he worked as a member of faculty in the Electronics and Microelectronics Division, Indian Institute of Information Technology (IIIT), Allahabad, India. From 2012 onwards, he has been working as a member of faculty in the School of Computing and Electrical Engineering (SCEE), Indian Institute of Technology (IIT), Mandi, (Himachal Pradesh), India. His current research interests include microelectronics circuits and system, CMOS device, fabrication and characterization, nano/microfabrication and design, polymer nanocomposite, sensors, photovoltaic, and self-assembly.